d. Detail of the research work duly signed by the applicant, for which the Sun Pharma Research Award is claimed, including references and illustrations (not to exceed 6000 words).

Toluidine Blue conjugated gold-silver nano-shells mediated photodynamic therapy to treat diabetic foot ulcer: A nano-phototheranostic approach

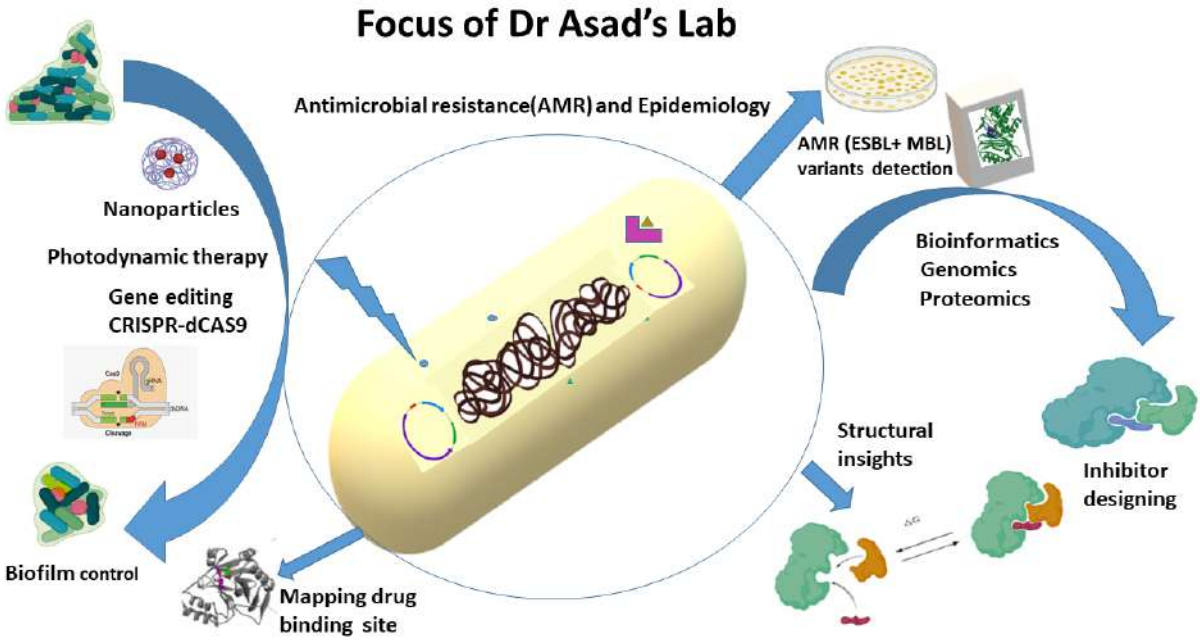

Synopsis

Diabetic foot infection caused by multidrug-resistant bacteria, is becoming serious problem. Moreover, polymicrobial biofilms contribute significantly to the persistent infections. In the present study, we investigated the effectiveness of novel toluidine blue conjugated chitosan coated gold-silver core-shell nanoparticles (TBO-chit-Au-AgNPs) mediated photodynamic therapy and demonstrate their use as a nontoxic antibacterial therapy to combat diabetic foot ulcer caused by multi-drug resistant strains both in monomicrobial and polymicrobial state of infection. In vitro efficacy of TBO-chit-Au-AgNPs mediated photodynamic therapy against polymicrobial biofilms was determined. Its therapeutic potential was validated in vivo type-2 DFU animal model. Cytokine's level was found reduced, using nano-phototheranostic approach, indicating infection control. Expression profile of growth factors confirmed both the pathogenesis and healing of DFU.

We conclude that TBO-chit-Au-AgNPs mediated PDT is a promising anti-bacterial therapeutic approach for healing of DFU caused by MDR bacterial strains.

Background

Type 2 diabetes mellitus (DM) has become an utmost health concern which comprised of 90-95% diabetes among worldwide population[1]. Nevertheless, immunocompromised patients identified with diabetes mellitus are more prone to be suffered from non-healing wounds[2]. It has also been reported that up to one-third of people with diabetes may develop foot ulcer during their lifetime and over 50% of these ulcers become infected. This challenge is further aggravated by the emergence of multidrug-resistance (MDR) strains induced diabetic foot infections (DFIs) which leads to increasing morbidity and mortality, and risk of lower extremity amputation (LEA) which causes low quality of life[3]. It has been stated earlier those biofilms intricate up to 65% of infections, leading to severe illness with a prolonged stay in hospital settings which may increase cost of treatment as well as mortality rate[4].

The most commonly found microorganisms which are isolated from patients with diabetic foot ulcer were reported as *Pseudomonas aeruginosa, Staphylococcus aureus, Escherichia coli, Enterococcus spp., Streptococcus spp., Proteus mirabilis* and anaerobes[5]. Among them, *S. aureus* and *P. aeruginosa* are the major cause of DFIs. For instance, polymicrobial, *S. aureus* and *P. aeruginosa* infections appear frequently in deep or chronic wounds[6,7]. The mutualistic and parasitic interactions cause synergistic association among the two species which led to the development of infections[8, 9]. Since no antibiotics are left to treat such infections therefore, the need of an hour is to search for alternative therapy.

These metal nanoparticles produce different kinds of intracellular reactive oxygen species (ROS) which damages microbial membrane and other cellular components, thereby causing cell death[10].

The antimicrobial actions of metal nanoparticles including gold and silver have already been established. Here, we initiated to fabricate a chitosan-coated gold nanoparticle (chit-AuNPs) as a core material[11], followed by the deposition of the silver shell. It is worth to mention that chitosan biopolymer act as an effective reducing and stabilizing agent as well as an external layer to provide the nanocomposites with several advantages[12]. Whereas, silver ions act upon various sites in microorganisms to cease their growth. Previously, it was shown that silver nanoparticles are generally liable for the contact killing of microorganisms[13]. We intend to conjugate chit-Au-AgNPs metal composite with a photosensitizer (TBO), which will further enhance the antibacterial efficacy of this nanocomposite and possibly eradicates infection caused by resistant bacteria. Toluidine blue O (TBO) is a cationic phenothiazine dye that has been well studied as an antibacterial photosensitizer. It departs a high quantum of cytotoxic singlet oxygen during photosensitization with 630 nm wavelength of light[14]. This approach is highly effective in killing MDR strains since microorganisms do not acquire resistance toward PDT[15].The use of TBO-chit-Au-AgNPs mediated PDT has not been reported yet. Therefore, we initiated this study to provide a novel approach toward potential applications of nano-phototheranostic complex, as a nontoxic antibacterial agent to combat DFU caused by multi-drug resistant bacterial strains.

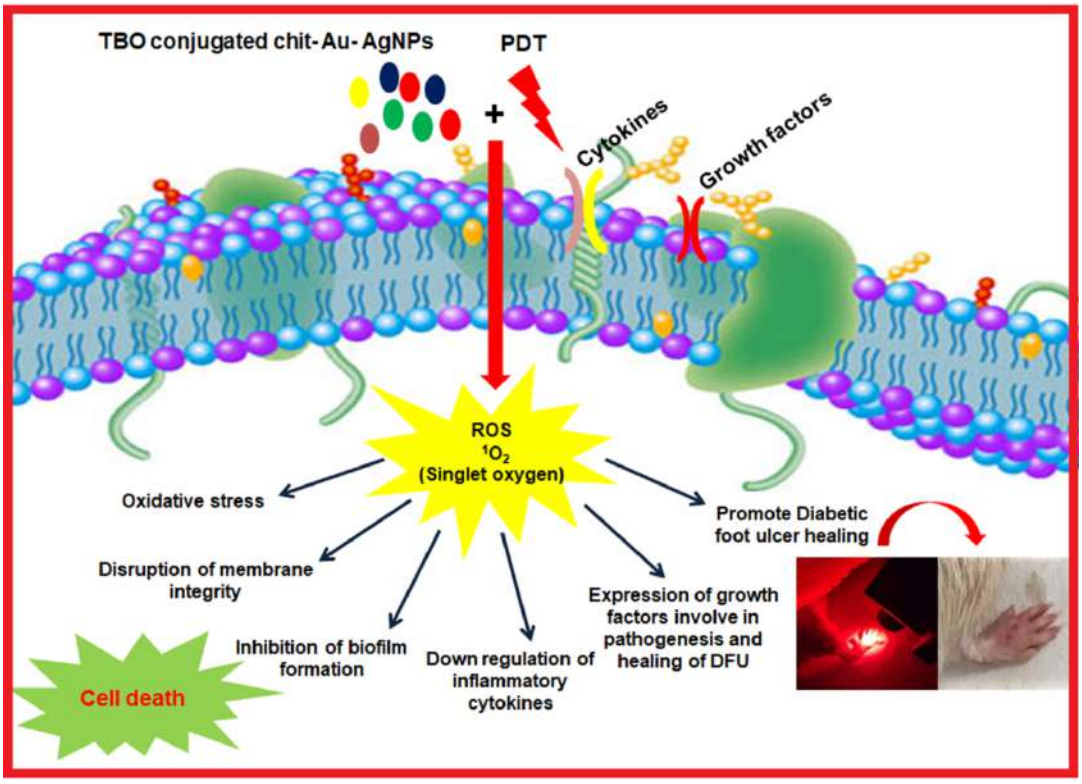

Figure 1. *Schematic representation of nanoparticle mediated antimicrobial photodynamic therapy against diabetic foot ulcer.*

Experimental data:

Synthesis and characterization of TBO-chit-Au-AgNPs

Chitosan-coated gold nanoparticles (chit-AuNPs, Figure.2A (a)) were synthesized as core materials to produce biocompatible gold-silver core-shell nanoparticles (chit-Au-AgNPs). The synthesized TBO-chit-Au-AgNPs were characterized by UV-spectroscopy, TEM, DLS and Zeta potential. Furthermore, we have performed elemental mapping of chit-Au-AgNPs using scanning electron microscopy (SEM) with energy dispersive X-ray spectrometry (EDS). The addition of TBO with chit-Au-AgNPs under dark conditions has led to the formation of TBO-chit-Au-AgNPs (Figure.2A (f)-green spectrum). The UV-visible spectrum of the synthesized chit-AuNPs (Figure.2A (f)-blue spectrum) exhibits a well-defined SPR band centered at 530 nm. After 60

minutes, occurrence of a new band takes place at 405 nm (Figure. 2A (f)-red spectrum) upon first addition of AgNO3 aliquots. The dark gold core and the brighter silver shell as observed in Figure.2A (b-d), was clearly distinguishable because of higher electronic density of gold than silver. Furthermore, Figure.2A (e) showed the presence of chitosan layer as a faint shadow which encapsulates the Au-AgNPs after their formation. Moreover, the result of scanning electron microscopy (SEM) with energy dispersive X-ray spectrometry (EDS) analysis (EDX) clearly shows the presence of Au, Ag and chitosan in pure form with weights of 13.26% Au, 9.98% Ag, 24.12% C and 52.64% O in the sample (Figure.2B-a, b, c, d and e). Besides, the average size of chit-AuNPs, chit-Au-AgNPs and TBO-chit-Au-AgNPs were found to be 129.4 nm, 131 nm, and 134 nm, respectively, as analyzed by dynamic light scattering (DLS) (Table.1). Changes in the polydispersity index (PDI) were also measured over this time. The PDI of chit-AuNPs, chit-Au-AgNPs and TBO-chit-Au-AgNPs remained low, indicating that there is least or no aggregation of particles. In addition, the result of zeta potential clearly illustrates chit-Au-AgNPs synthesized through stepwise addition of AgNO3 retains their positive zeta potential of +37.6 mV, which shows that the polymeric coating is well-preserved all through the formation of core-shell nanoparticles (chit-Au-AgNPs).. Even after the addition of TBO, chit-Au-AgNPs exhibited strong positive zeta potential of +41.2 mV, suggesting the stability and biocompatibility of synthesized TBO-chit-Au-AgNPs (Table**.1**).

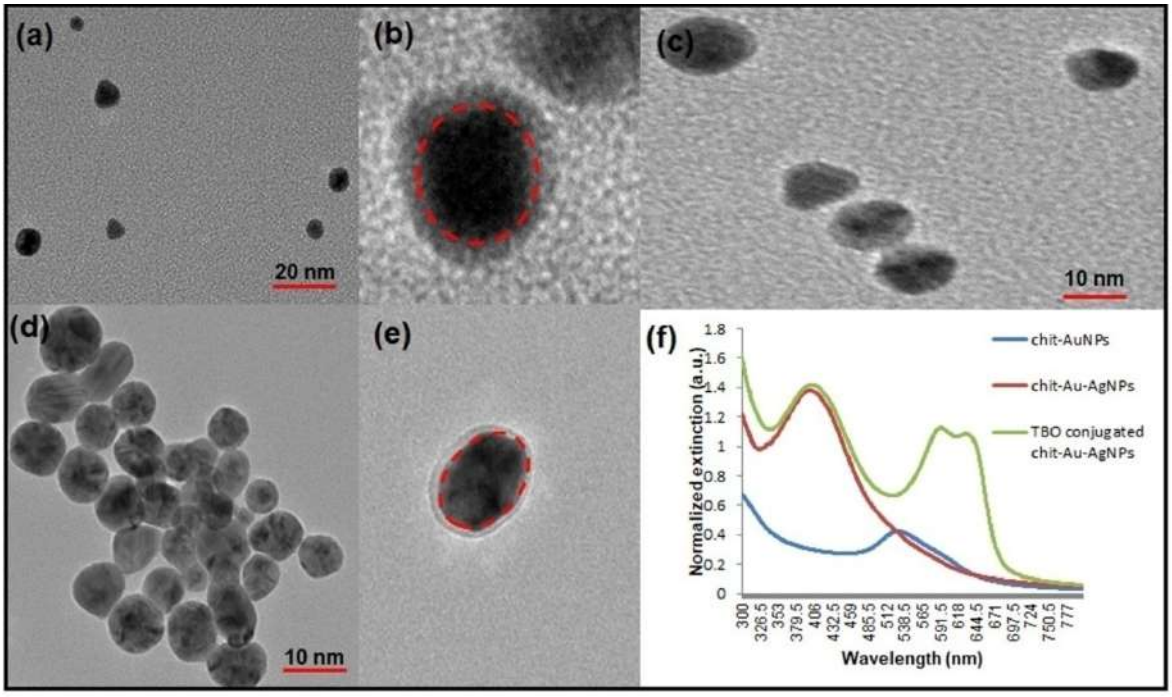

Figure 2. Characterization of nanoparticles: A. *(a) TEM image of spherical chit-AuNPs. (b)-(d) TEM images of chit-Au-AgNPs after additions of AgNO3 aliquots. The interface between the Au-core and the Ag-shell was marked by a red dashed line in figure 1(b). (e) A closer view of an Au–AgNP coated by a chitosan layer. (g) UV-Vis absorption spectra of chit-AuNPs, chit-Au-AgNPs and TBO-chit-Au-AgNPs.*

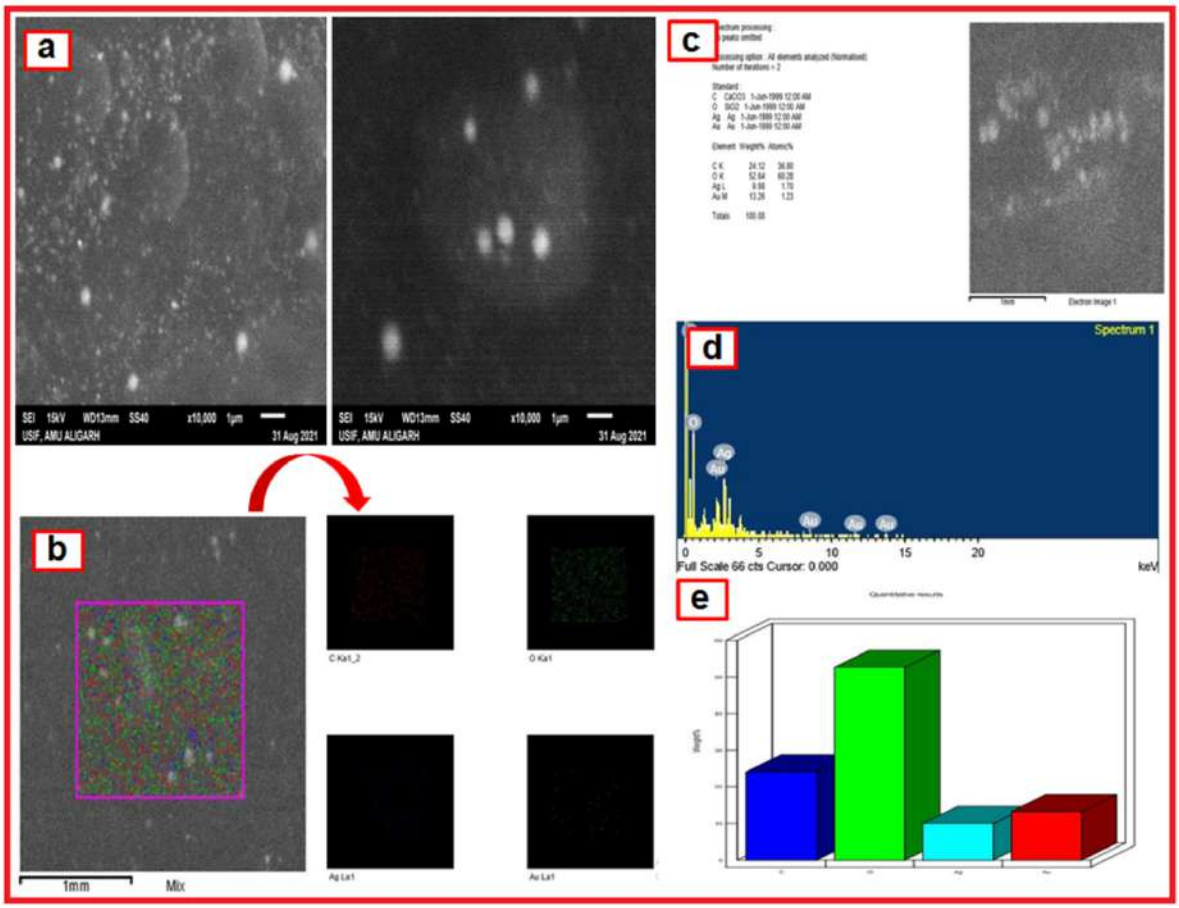

***Figure** 2B. (a) Scanning electron microscopy (SEM) images of chit-Au-AgNPs. (b)-(e) Energy dispersive X-ray spectrometry (EDS) profile of chit-Au-AgNPs and quantitative analysis.*

Effect of TBO-chit-Au-AgNPs mediated photodynamic therapy on cellular toxicity

The relative cellular viability of L929 fibroblast cells in the presence of various concentrations (0.25 mM, 0.5 mM and 1 mM) of TBO-chit-Au-AgNPs with and without laser irradiation is shown in Figure.3. Almost 65.12 % and 74.32 % viability were observed at our tested concentration (0.5 mM) with and without laser irradiation respectively. Thus, the concentration of the TBO-chit-Au-AgNPs and exposure time (100 J/cm^2) of red laser light used in this study was found to be non-toxic.

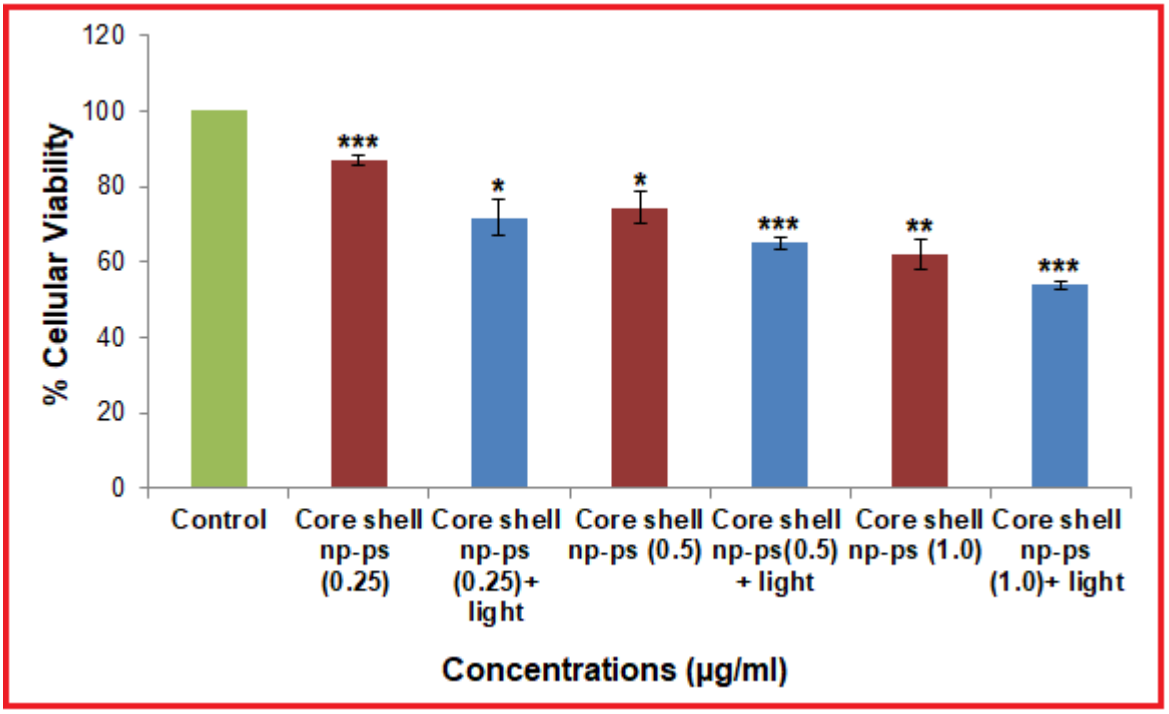

Figure 3. Cytotoxicity assay: *Percentage viable cells as measured after 24 hrs, after treatment with TBO-chit-Au-AgNPs in absence and presence of laser irradiation.*

In vitro anti-bacterial activity of TBO-chit-Au-AgNPs mediated PDT on monomicrobial and polymicrobial biofilms

After incubation for 24 h, the resulting monomicrobial biofilms showed 2.76 log10 CFU/mL reduction of S.aureus and 2.17 log10 CFU/mL reduction of P. aeruginosa in the group treated with TBO-chit-Au-AgNPs only. While, 2.15 log10 CFU/mL reduction was seen in polymicrobial biofilms (Figure.4). A substantial reduction in bacterial load was achieved when monomicrobial and polymicrobial biofilms of S.aureus and P. aeruginosa treated with TBO-chit-Au-AgNPs and subsequently to 100 J/cm^2 of laser irradiation. A 6.86 $\log_{10}$CFU/mL and 5.4 $\log_{10}$ CFU/mL reduction was found in the monomicrobial biofilm of *S.aureus* and *P.aeruginosa*, respectively, whereas 5.31 $\log_{10}$ CFU/mL reductions were observed in the polymicrobial biofilms of both the species (**Figure 4**). The bacterial load reduction in the

polymicrobial biofilms of *S.aureus* and *P. aeruginosa* was found to be lower than monomicrobial biofilms of both the species after nano-photodynamic therapy

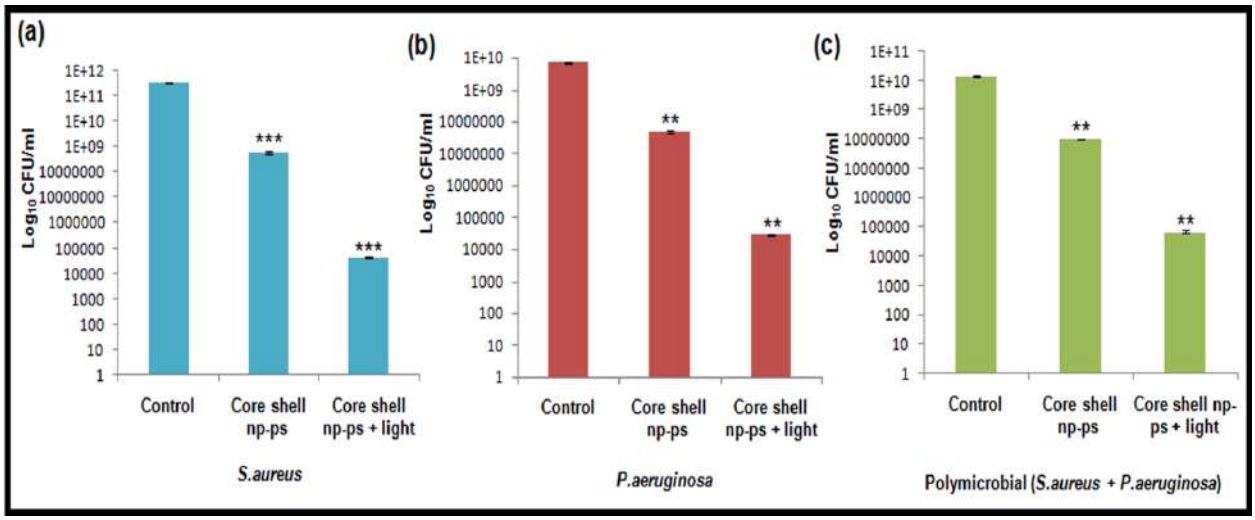

Figure 4. In vitro colony formation: *(a) Monomicrobial S. aureus, (b) Monomicrobial P. aeruginosa and (c) Polymicrobial S. aureus + P. aeruginosa colonies after incubation with TBO-chit-Au-AgNPs or TBO-chit-Au-AgNPs and/or irradiation with 630 nm laser for 12 min and 50 seconds which corresponds to 100 Jcm^{-2} .*

Generation of reactive oxygen species and singlet oxygen quantification

Our data showed increase production of intracellular ROS in TBO-chit-Au-AgNPs mediated photodynamic therapy treated group as compared to TBO-chit-Au-AgNPs alone, both in monomicrobial as well as in polymicrobial biofilms. Whereas, no ROS production was seen in the group treated with light only. Thus, we conclude that the potentiation of killing or enhanced antibacterial activity is dependent upon the generation of ROS (**Figure.5 a,b,c**). However, the photoinactivation was found to be more pronounced in monomicrobial biofilm than polymicrobial biofilms of both the species.

Furthermore, to confirm the type of phototoxicity, we have measured the degradation rate of AMDA. Since, the amount of ROS produced is directly proportional to the bacterial cell death;

our data revealed enhanced production of 1O2 in TBO-chit-Au-AgNPs mediated PDT treated group as compared to control and only TBO-chit-Au-AgNPs treated groups (Figure.5 d,e,f). This confirmed that type II photochemistry is the major photochemical reaction involved in TBO-chit-Au-AgNPs mediated photodynamic therapy on monomicrobial and polymicrobial biofilms.

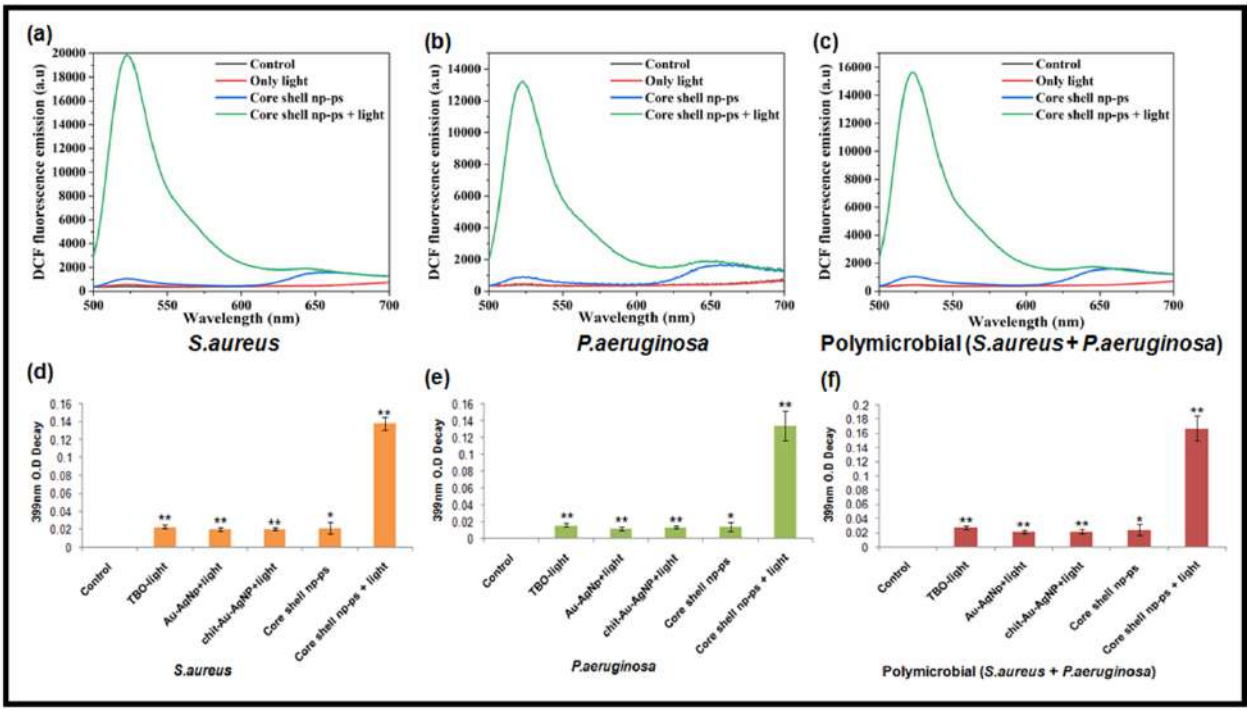

Figure 5. *Detection of total reactive oxygen species (a)-(c) and quantification of singlet oxygen (d)-(f) in monomicrobial S. aureus, monomicrobial P. aeruginosa and (c) polymicrobial S. aureus + P. aeruginosa biofilms in the groups of control, TBO-chit-Au-AgNPs and TBO-chit-Au-AgNPs + laser. 630 nm laser (100 Jcm-2, 12 min and 50 seconds) were used in the corresponding laser group.*

Anti-biofilm effect of TBO-chit-Au-AgNPs mediated photodynamic therapy

The result of crystal violet assay showed 28.02 % and 34. 04% reduction in the monomicrobial *S.arureus* and *P.aeruginosa* biofilm formation, respectively, after treatment with, exclusively TBO-chit-Au-AgNPs, whereas 45. 89% of polymicrobial biofilms were found to be reduced.

Moreover, significant decrease in microbial biomasses was found in TBO-chit-Au-AgNPs mediated photodynamic therapy treated group as compared to control and exclusively TBO-chit-Au-AgNPs treated groups. Our data showed 72.82% and 59. 15 % reduction in the monomicrobial biofilm of S.aureus and P.aeruginosa, respectively, while 67.69% reduction was found in the polymicrobial biofilms after treatment with TBO-chit-Au-AgNPs and subsequently to 100 J/cm2 of laser irradiation (Figure.6 a,b,c). Besides this, EPS production was reduced by 13.65% and 30.71% in monomicrobial biofilm of S.aureus and P.aeruginosa, whereas 17.16 % in polymicrobial biofilms after being treated with exclusively TBO-chit-Au-AgNPs. While, 51.55% and 42.71% EPS reduction was achieved in monomicrobial biofilm of S.aureus and P.aeruginosa, respectively, after being photoinactivated by TBO-chit-Au-AgNPs. However, 40.9% reduction was seen in polymicrobial biofilms as shown in **Figure.6 d,e,f**.

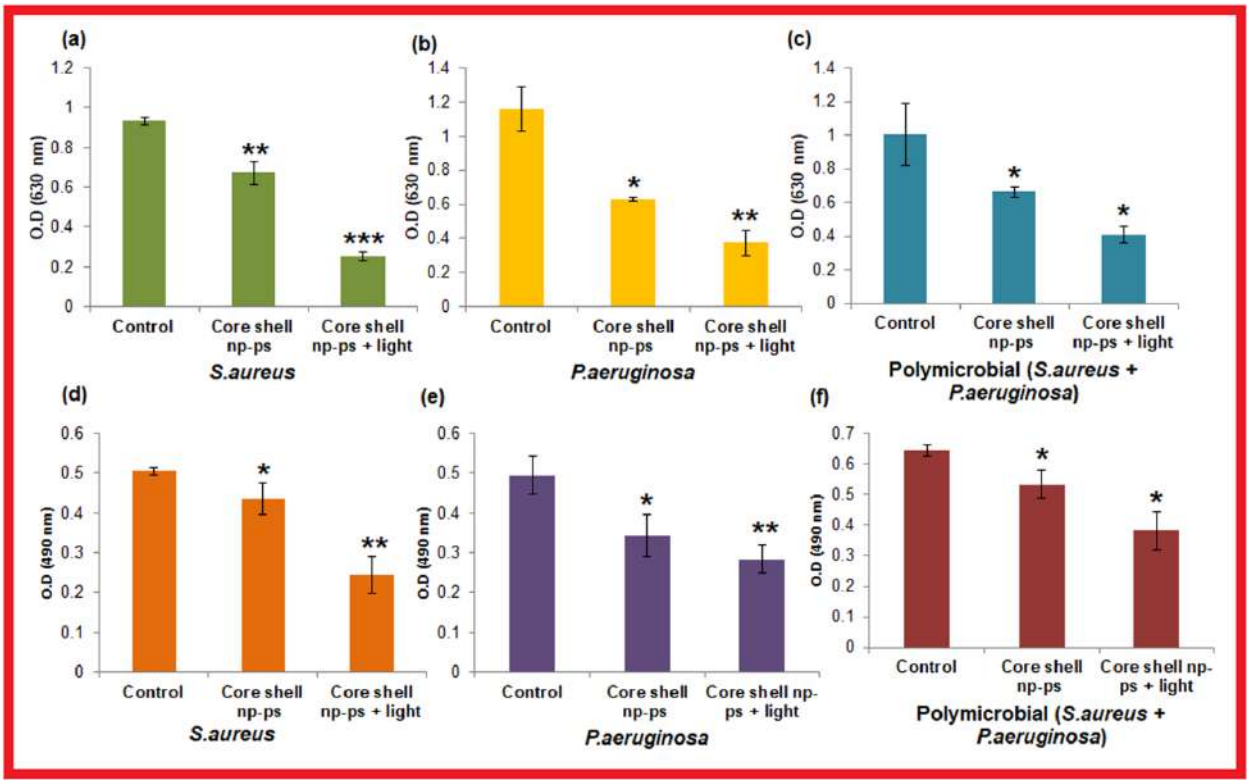

Figure 6. Antibiofilm forming ability of *TBO-chit-Au-AgNPs mediated photodynamic therapy: (a)-(c) represents inhibitory effect of TBO-chit-Au-AgNPs mediated PDT on monomicrobial S. aureus, monomicrobial P. aeruginosa and polymicrobial S. aureus + P. aeruginosa biofilms, respectively as quantified by Crystal violet assay. Absorbance was measured at 630 nm. Figure (d) - (f) showed effect of TBO-chit-Au-AgNPs mediated PDT on extracellular polysaccharide substance (EPS) reduction as quantified by Congo-red assay.*

Visualization of biofilms architect after TBO-chit-Au-AgNPs mediated photodynamic therapy

Confocal and scanning electron microscopy was performed to examine the morphological changes in bacteria after TBO-chit-Au-AgNPs mediated photodynamic therapy, and to elucidate the underlying anti-bacterial mechanisms. CLSM micrographs illustrate greater disruption of polymicrobial biofilms of S.aureus and P. aeruginosa in TBO-chit-Au-AgNPs mediated photodynamic therapy treated group (Figure.7i) as compared to control (Figure.7c) and exclusively TBO-chit-Au-AgNPs (Figure.7 f). Moreover, the monomicrobial biofilms of S. aureus and P. aeruginosa was more severely disrupted, almost all the bacterial cells in the biofilms were found dead in TBO-chit-Au-AgNPs mediated PDT group (Figure.7-gand h), as compared to control (Figure. 7-a and b) and exclusively TBO-chit-Au-AgNPs treated group (Figure.7-d and e). Thereby, demonstrating strong antibiofilm action of TBO-chit-Au-AgNPs mediated photodynamic therapy. TBO-chit-Au-AgNPs treatment reduced the thickness of the biofilm to approximately 4 µm and 3 µm in monomicrobial biofilm of S. aureus and P. aeruginosa, respectively, as compared to control (6 µm and 4 µm, respectively). However, the thickness was found to be 2.5 µm and 2 µm, respectively in TBO-chit-Au-AgNPs mediated PDT treated group, suggesting prevalence of dead cells throughout the biofilm. Likewise, polymicrobial biofilm of S. aureus and P. aeruginosa treated with TBO-chit-Au-AgNPs mediated PDT decreases the thickness of the biofilm to approximately 3 µm as compared to control (8 µm) and TBO-chit-Au-AgNPs alone (6 µm). This observation was further supported

by the scanning electron microscopy. The control groups of monomicrobial as well as polymicrobial *S. aureus* and *P. aeruginosa* biofilms displayed highly dense and compact microbial cells (Figure. 8-a, b, c). While, after treatment with TBO-chit-Au-AgNPs followed by exposure to 100 J/cm2 of laser light, the density of the microbial cells in the monomicrobial as well as in the polymicrobial biofilms of both the species decreases significantly (Figure.8-g, h, i). Less reduction was observed in only TBO-chit-Au-AgNPs treated groups (Figure.8-d, e, f). Furthermore, TBO-chit-Au-AgNPs mediated PDT treated groups showed detrimental effects on cell wall with significant dispersion of the cells leading to leakage of the cellular content, thus obliterating the structural integrity of the biofilm.

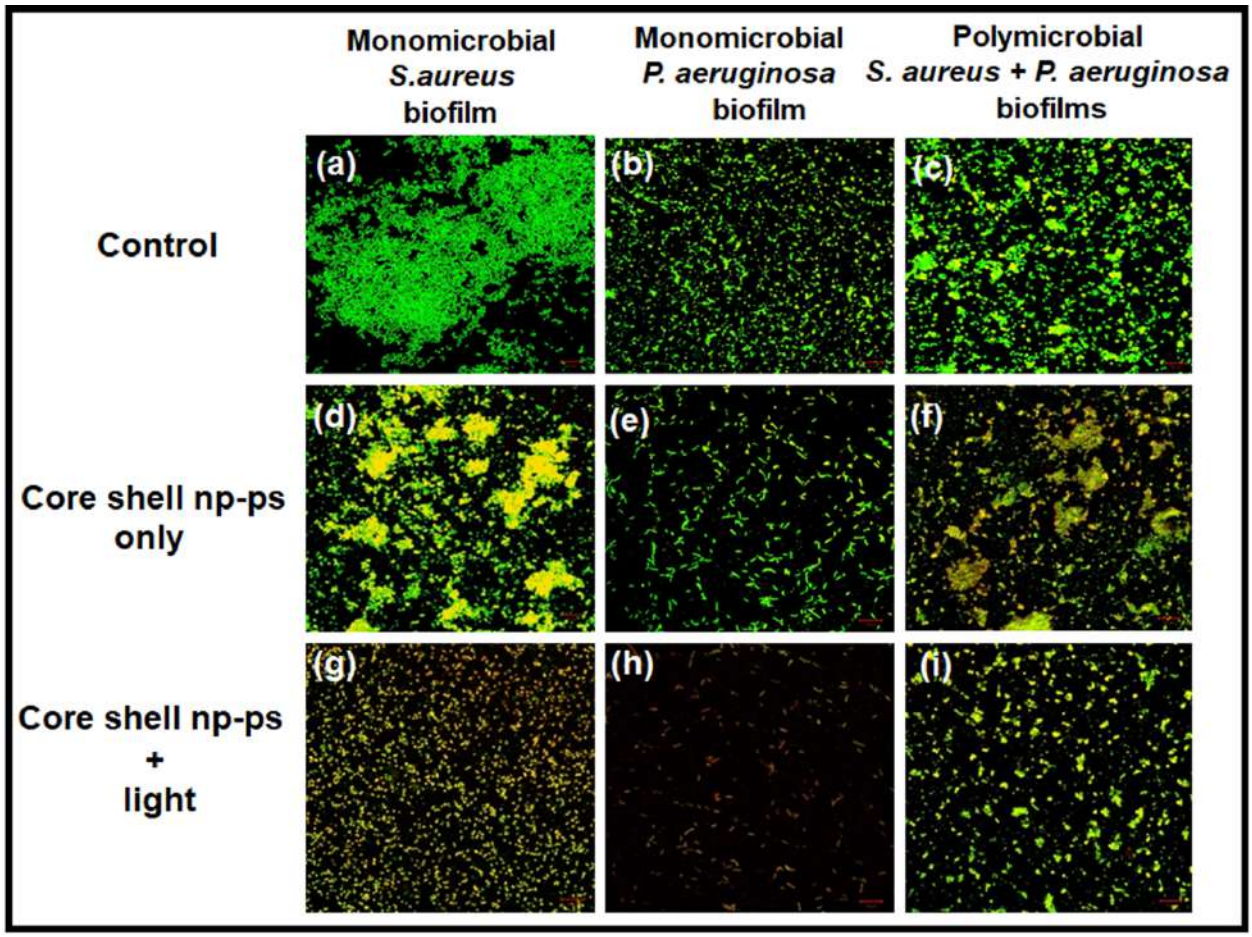

Figure 7. Fluorescence-based live/dead analysis of monomicrobial S. aureus, *monomicrobial P. aeruginosa and polymicrobial S. aureus + P. aeruginosa biofilms: Representative fluorescence images of SYTO 9 (live, green) and PI (dead, red) stained bacteria in the groups of control (a)-(c), TBO-chit-Au-AgNPs treated (d)- (f) and TBO-chit-Au-AgNPs + laser treated (g)- (i). 630 nm laser (100 Jcm-2, 12 min and 50 seconds) were used in the corresponding laser group. Scale bar = 10 µm.*

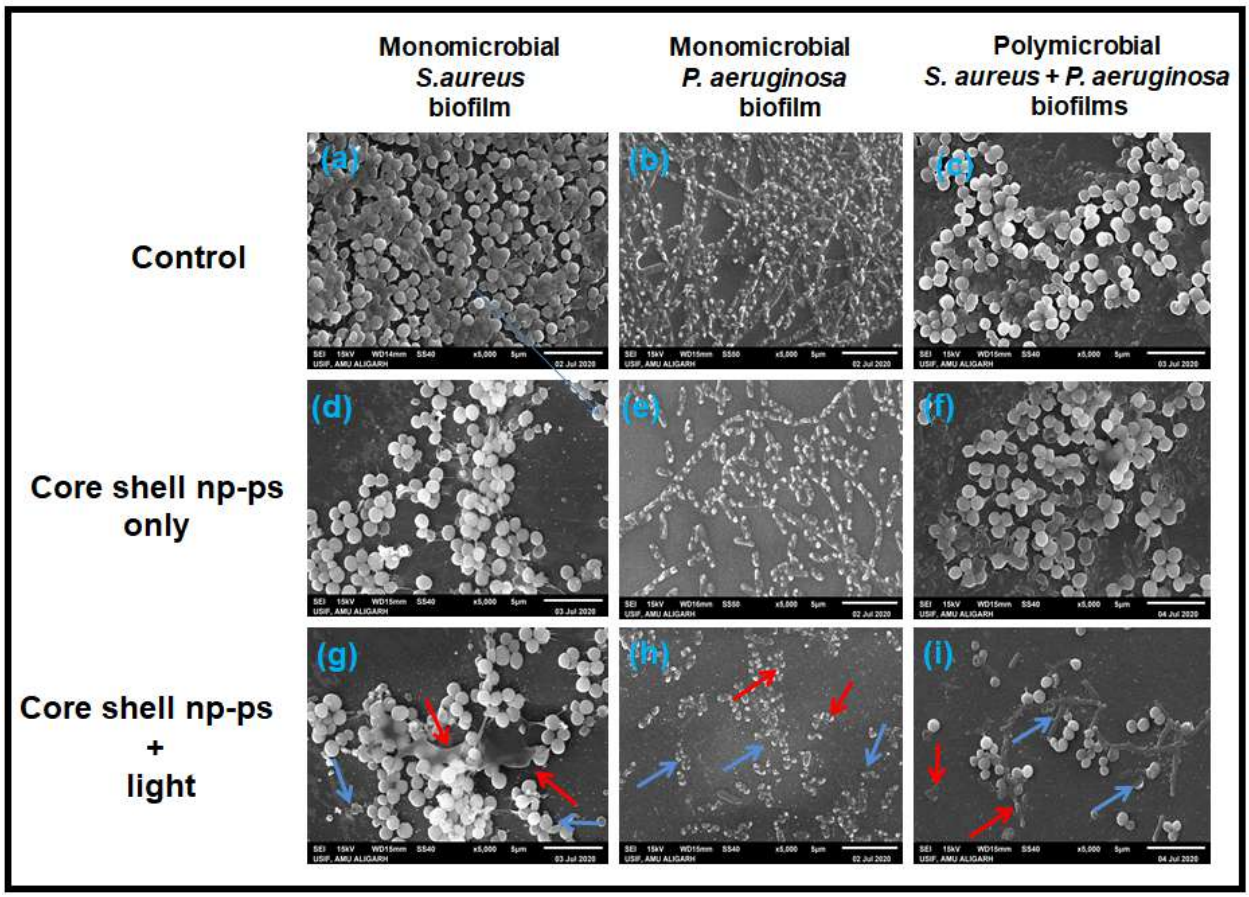

Figure 8. *Scanning electron microscopy (SEM) images of monomicrobial S. aureus, monomicrobial P. aeruginosa and polymicrobial S. aureus + P. aeruginosa biofims of control (a)-(c), TBO-chit-Au-AgNPs treated (d)-(f) and TBO-chit-Au-AgNPs + laser treated (g)-(i). 630 nm laser (100 Jcm^{-2}, 12 min and 50 seconds) were used in the corresponding laser group. Red arrow indicates bursting and release of cellular constituents while blue arrow* indicates complete rupturing of the cells.

In vivo efficacy of TBO-chit-Au-AgNPs mediated photodynamic therapy in the treatment of Diabetic Foot Ulcer

The efficacy of TBO-chit-Au-AgNPs mediated photodynamic therapy in healing of diabetic foot ulcer in male wistar rats was checked. Streptozotocin (STZ)-induced type 2 DM rats with blood glucose level higher than 300mg/dl were developed and used for further study (Table.2). Our result showed that daily topical exposure of TBO-chit-Au-AgNPs followed by light irradiation led to the marked reduction of *S. aureus* and *P. aeruginosa* colonization in diabetic foot ulcer rats within 7 days, starting from the day 3 post infection (**Figure.9 and Figure.10 A, B, C**). Furthermore, histopathological analysis of untreated monomicrobial and polymicrobial DFU (**Figure.11B-d, e, f**) revealed dense population of inflammatory cells with focal neutrophilic infiltrate attached to the stratified squamous epithelium as compared to control, diabetic (**Figure.11A**) and ulcerated groups (**Figure.11B-a,b,c**). In addition, the ulcerated squamous epithelium in untreated DFU rats showed decrease collagenization with few basal thin capillaries and mild fibrosis. This confirms the incidence of an ongoing infection. However, the ulcer sites of the TBO-chit-Au-AgNPs treated group showed acanthotic (thickened) squamous epithelium with moderate fibrosis. Besides this, restorative ulcer was observed with focal moderately thick collagen fibers and few compressed capillaries (Figure.11B-g, h, i). In comparison, TBO-chit-Au-AgNPs mediated photodynamic therapy treated DFU showed intact stratified squamous epithelium with marked neo-angiogenesis and collagenization (**Figure.11B-j, k, l**).

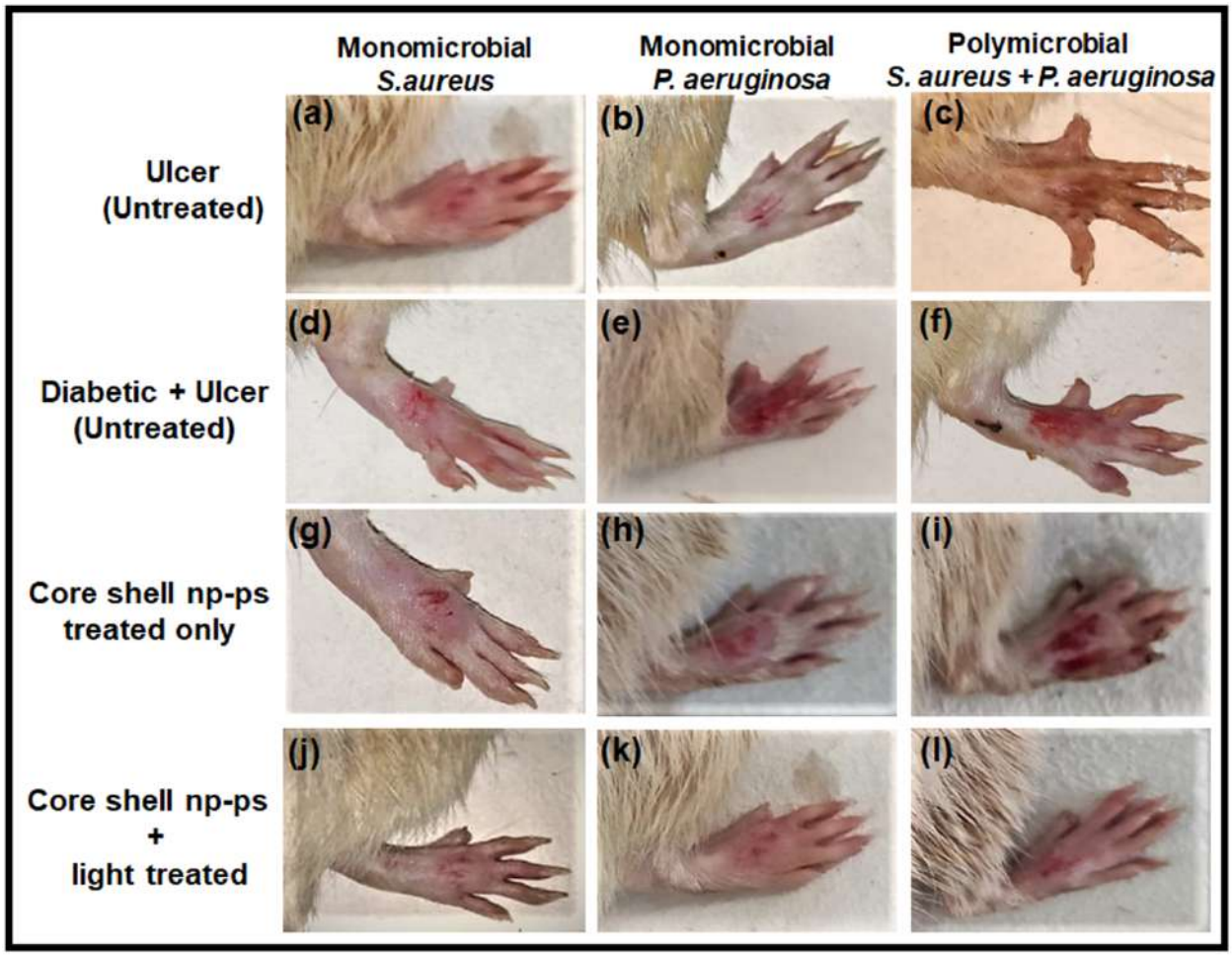

Figure 9. Photographic image of wistar rats*: Untreated foot ulcer (a)-(c), untreated foot ulcer with diabetes (d) - (f), diabetic foot ulcer after applying TBO-chit-Au-AgNPs (g)-(i) and diabetic foot ulcer after treatment with TBO-chit-Au-AgNPs mediated PDT.*

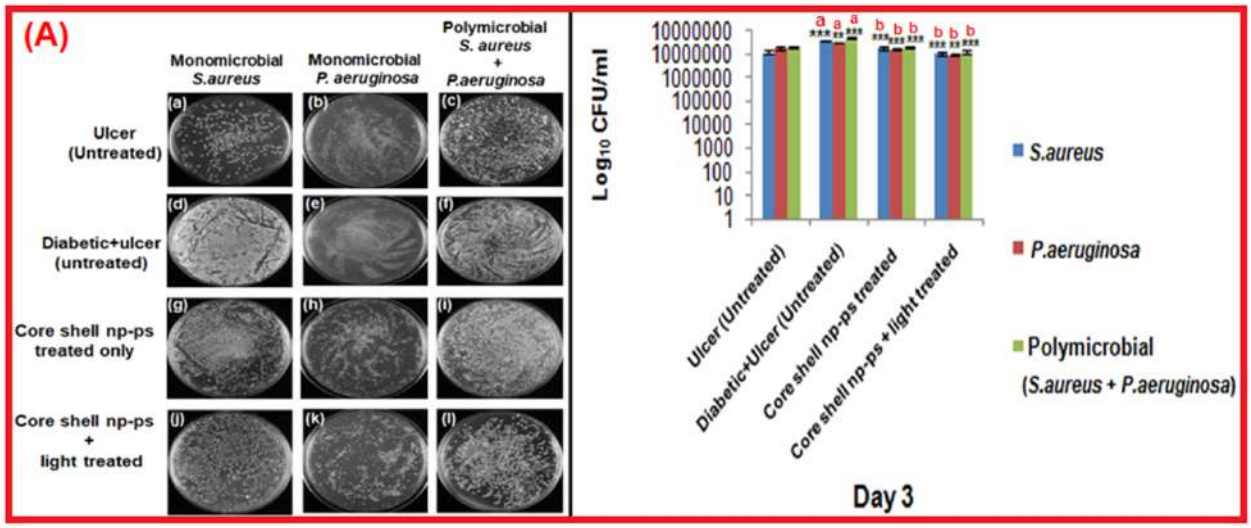
(A)
Monomicrobial S.aureus
Monomicrobial P. aeruginosa
Polymicrobial S. aureus + P.aeruginosa
Ulcer (Untreated)
Diabetic+ulcer (untreated)
Core shell np-ps treated only
Core shell np-ps + light treated
Log10 CFU/ml
10000000
1000000
100000
10000
1000
100
10
1
Ulcer (Untreated)
Diabetic+Ulcer (Untreated)
Core shell np-ps treated
Core shell np-ps + light treated
S.aureus
P.aeruginosa
Polymicrobial (S.aureus + P.aeruginosa)
Day 3

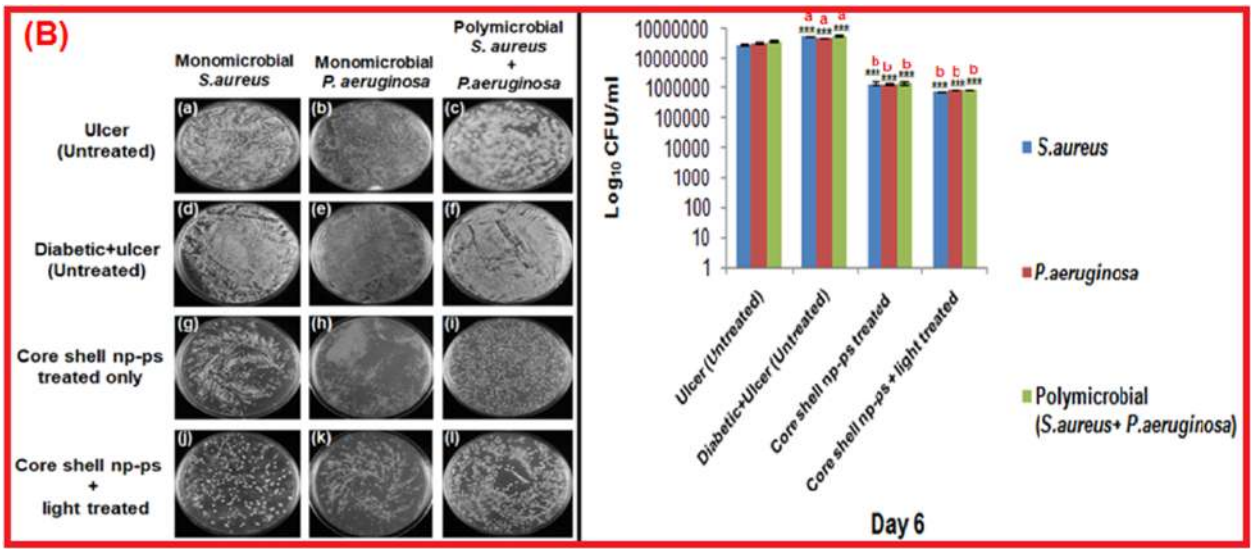
(B)
Monomicrobial S.aureus
Monomicrobial P. aeruginosa
Polymicrobial S. aureus + P.aeruginosa
Ulcer (Untreated)
Diabetic+ulcer (Untreated)
Core shell np-ps treated only
Core shell np-ps + light treated
Log10 CFU/ml
10000000
1000000
100000
10000
1000
100
10
1
Ulcer (Untreated)
Diabetic+Ulcer (Untreated)
Core shell np-ps treated
Core shell np-ps + light treated
S.aureus
P.aeruginosa
Polymicrobial (S.aureus+ P.aeruginosa)
Day 6

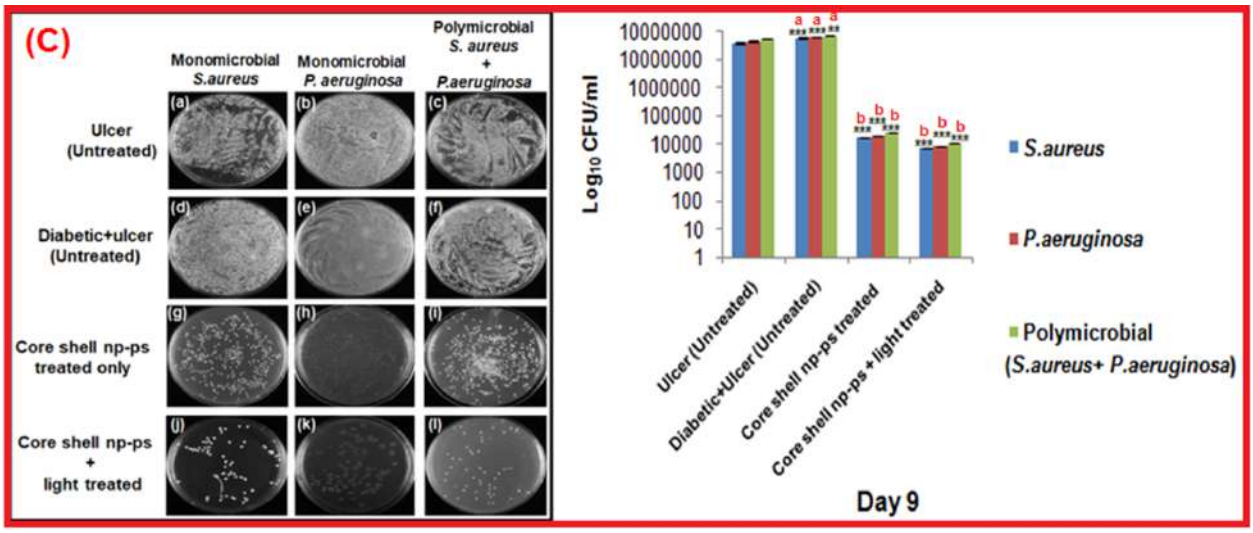
(C)
Monomicrobial S.aureus
Monomicrobial P. aeruginosa
Polymicrobial S. aureus + P.aeruginosa
Ulcer (Untreated)
Diabetic+ulcer (Untreated)
Core shell np-ps treated only
Core shell np-ps + light treated
Log10 CFU/ml
10000000
1000000
100000
10000
1000
100
10
1
Ulcer (Untreated)
Diabetic+Ulcer (Untreated)
Core shell np-ps treated
Core shell np-ps + light treated
S.aureus
P.aeruginosa
Polymicrobial (S.aureus+ P.aeruginosa)
Day 9

Figure 10. In vivo antibacterial effect of TBO-chit-Au-AgNPs mediated photodynamic therapy in DFU rats: *(A) CFU/ml at day 3 post ulceration, (B) CFU/ml at day 6 post ulceration and treatment, (C) CFU/ml at day 9 post ulceration and treatment.*

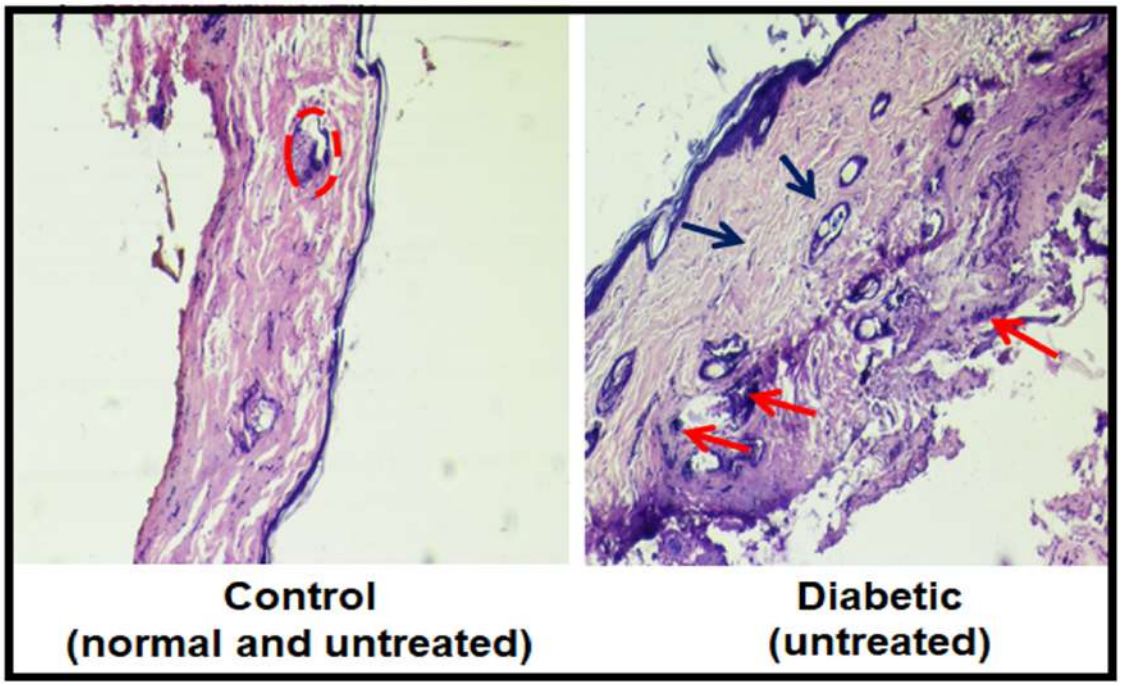

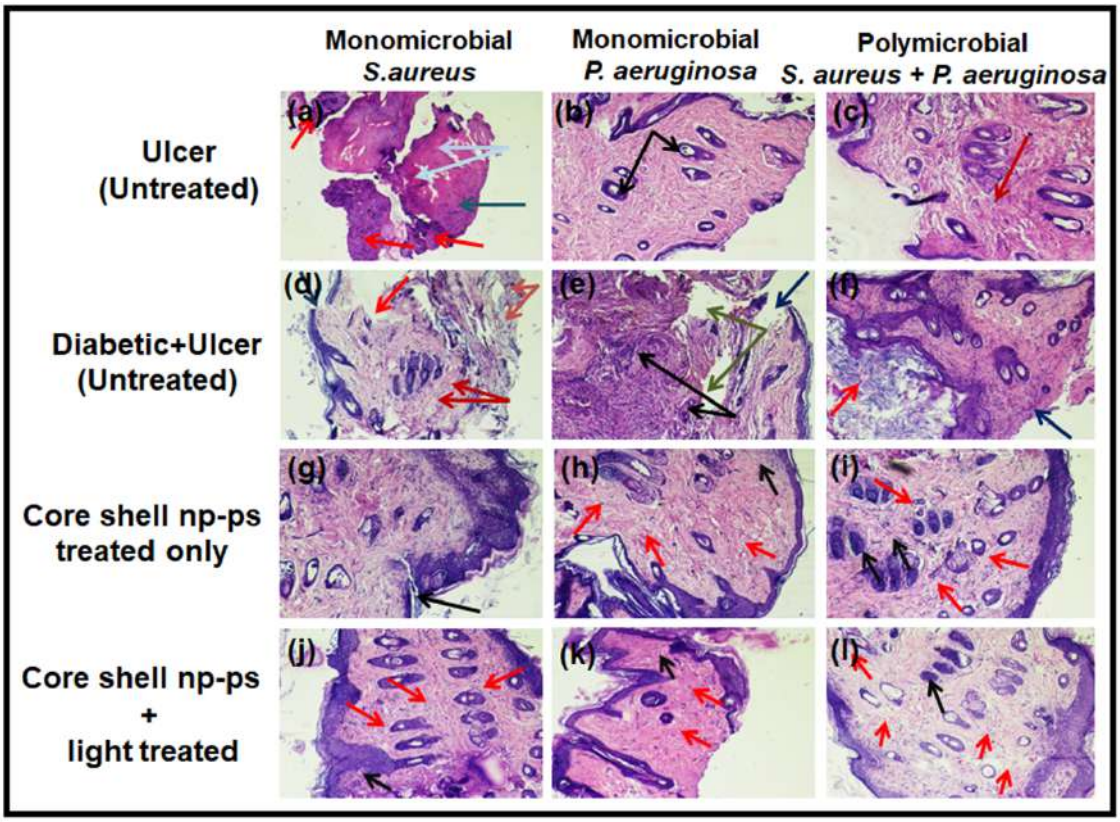

Figure 11. Hematoxylin and Eosin (H& E) (x 10X) staining to examine response to microorganism of: (A) *Control and diabetic rats,* ***(B)*** Ulcerated rats (untreated):figure (a)-(c), DFU rats (untreated): figure (d)-(f), DFU *rats treated with TBO-chit-Au-AgNPs: figure (g)-(i) and DFU rats treated with TBO-chit-Au-AgNPs + laser: figure (j)-(l).*

Effect of TBO-chit-Au-AgNPs mediated photodynamic therapy on growth factors and inflammatory cytokines

The expression levels of growth factors and cytokines in control (normal) rats were compared with diabetic and non-diabetic rats with healed (treated) and unhealed (untreated) ulcers.

We have found that failure of an ulcer to heal in diabetic rats was linked with an increased level of pro-inflammatory cytokines, such as IL-6 and TNF-α. Furthermore, the expression levels of pro-inflammatory cytokines were significantly higher in DFU rats with polymicrobial infections as compared to DFU rats with monomicrobial infection. However, decreased levels

of these cytokines were found in TBO-chit-Au-AgNPs mediated photodynamic therapy treated groups as compared to control, untreated and only TBO-chit-Au-AgNPs treated groups, implying restoration of immunosuppression (Figure.12-a and b). In addition, our data demonstrated significantly higher levels of EGF and VEGF in all those groups of rats whose ulcers healed as compared to those groups whose ulcers did not healed (**Figure.12-c and d**). However, their expression level was found to be lower in DFU rats with polymicrobial infections than that of monomicrobial infection, as the severity of infection was found to be more in polymicrobial state of infection. Besides this, elevated level of TGF-β-1 was found in all diabetic groups (with and without foot ulcer) (**Figure.12e**). Moreover, we have found expression levels of TGF-β-1 were significantly higher in diabetic rats with polymicrobial infections as compared to monomicrobial infection. In addition, IGF-1 level was found to be lower in diabetic rats as compared to non-diabetic and control rats. However, considerable decrease was found in DFU rats with polymicrobial infections (Figure.12f). Hence, the data suggest that TBO-chit-Au-AgNPs mediated PDT promotes healing in DFU rats through significantly reducing cytokine production while elevating EGF and VEGF levels by regulating the expression of TGF-β-1 and IGF-1.

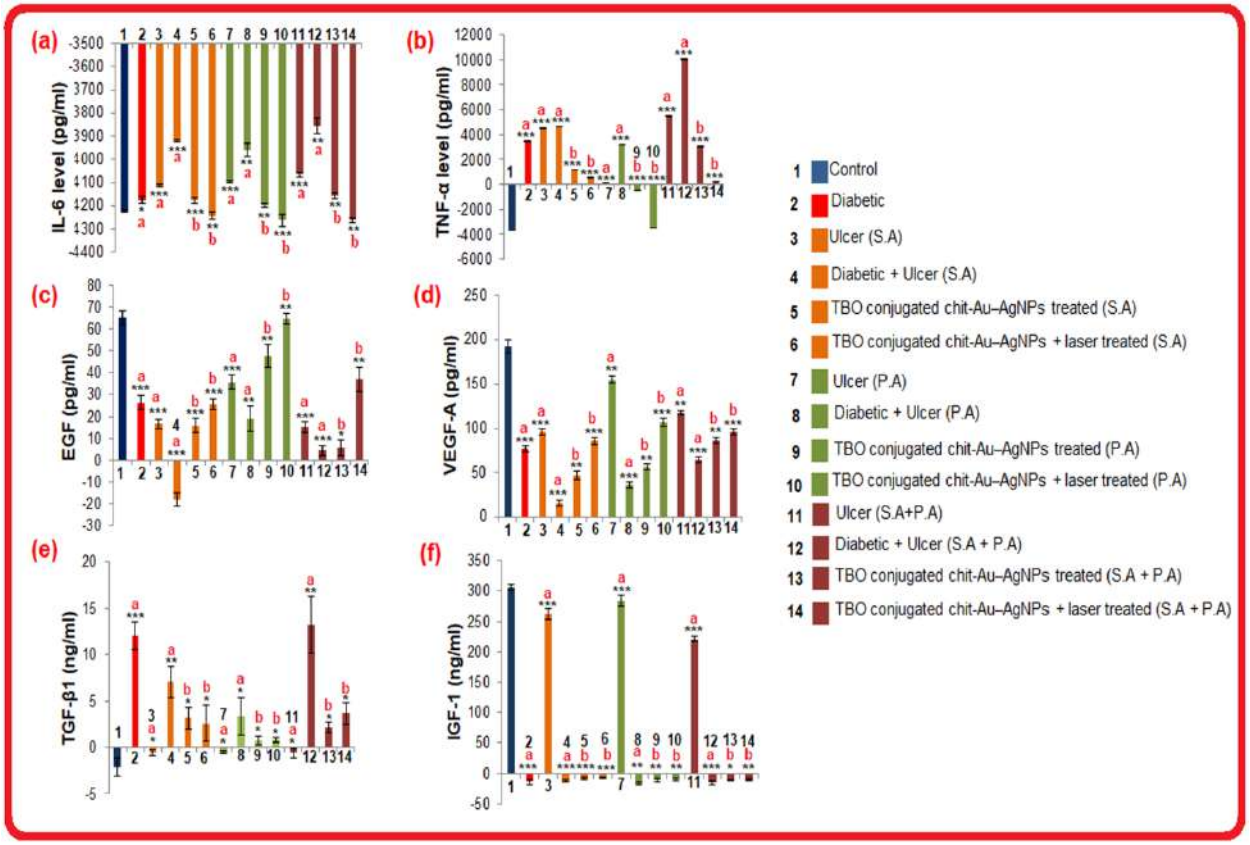

Figure 12. Effect of TBO-chit-Au-AgNPs mediated photodynamic therapy on pro-inflammatory cytokines and growth factors levels in Control rats, STZ induced diabetic rats (untreated), Ulcerated rats (untreated), DFU rats (untreated), DFU rats treated with TBO-chit-Au-AgNPs, DFU rats treated with TBO-chit-Au-AgNPs + laser: (a) IL-6 level, (b) TNF-α level, (c) EGF level , (d) VEGF-A level, (e) TGF-β1 level and (f) IGF-1 level. Each bar represents mean ± SD of 4 rats.

Discussion

Type 2 diabetes mellitus has become an utmost health concern which comprised of 90-95% diabetes among worldwide population[1]. It has also been reported that up to one-third of people with diabetes may develop foot ulcer during their lifetime and over 50% of these ulcers become infected. This challenge is further aggravated by the emergence of multidrug-resistance (MDR) strains induced diabetic foot infections (DFIs) which leads to increasing morbidity and mortality, and risk of lower extremity amputation (LEA) which causes low quality of life[3].

Majority of these infections are now being caused by *Pseudomonas aeruginosa, Staphylococcus aureus, Escherichia coli, Enterococcus spp., Streptococcus spp., Proteus mirabilis* and anaerobes[5].

S. aureus and *P. aeruginosa* are two versatile bacterial pathogens that are frequently found together in chronic wound infections[6]. Polymicrobial (mixed microbial culture) *S. aureus* and *P. aeruginosa* infections are more virulent and/or result in worse outcomes than the single infections caused by either species[5], leading to the formation of more resistant biofilms, which are difficult to be eradicated. In this regard, nanoparticle mediated photodynamic therapy emerged as an ideal candidate to meet such requirements.

Recently, chitosan coated gold-silver core-shell nanoparticles (chit-Au-AgNPs) was developed and labeled with para-mercaptobenzoic acid (4MBA) to demonstrate their ability to perform as SERS nanotags inside of human ovarian adenocarcinoma cells (NIH: OVCAR-3) under multiple excitation wavelengths[12]. Here, chit-Au-AgNPs were used for the first time in association with TBO.

Earlier studies have shown that photosensitizer activity is significantly improved when combine with nanoparticles[15]. Our study was planned to investigate the effectiveness of novel toluidine blue conjugated gold-silver core-shell nanoparticles (TBO-chit-Au-AgNPs) mediated photodynamic therapy and demonstrate their use as a nontoxic antibacterial therapy to combat diabetic foot ulcer (DFU) caused by multi-drug resistant strains both in monomicrobial and polymicrobial state of infection.

The synthesized TBO-chit-Au-AgNPs were characterized by UV-spectroscopy, TEM, scanning electron microscopy (SEM) with energy dispersive X-ray spectrometry (EDS), DLS

and Zeta potential. The UV-visible spectrum of the synthesized chit-AuNPs (Figure.2A (f)-blue spectrum) exhibits a well-defined SPR (surface plasmon resonance) band centered at 530 nm. For instance, occurrence of a new band takes place at 405 nm (Figure.2A (f) - red spectrum) upon first addition of AgNO3 aliquots. This spectral profile has already been reported in previous studies and it confirms the successful synthesis of a thin silver layer on the surface of the gold core16. The morphological progression of core-shell nanoparticles (chit-Au-AgNPs) was further confirmed by TEM. The dark gold core and the brighter silver shell as observed in Figure.2A (b-d), was clearly distinguishable because of higher electronic density of gold than silver. Furthermore, Figure.2A (e) showed the presence of chitosan layer as a faint shadow which encapsulates the Au-AgNPs after their formation. This foremost result demonstrated not only the effective synthesis of Au-AgNPs, but also their steadiness and bio-compatibilization, which are required essentially for the use of this nanoconjugate in biological systems. We next performed elemental mapping to verify the presence of gold and silver using scanning electron microscopy (SEM) with energy dispersive X-ray spectrometry (EDS). The result confirms the formation of chit-Au-Ag nanocomposites with no additional impurities as detected in the EDS (Figure.2B- a, b, c, d and e). Changes in the polydispersity index (PDI) were also measured over this time. The PDI of chit-AuNPs, chit-Au-AgNPs and TBO-chit-Au-AgNPs remained low, indicating that there is least or no aggregation of particles (**Table 1**). We have also measured the surface zeta potential to further confirm about the stability of nanoparticles. Our data demonstrated strong positive zeta potential of chit-Au-AgNPs (+41.2 mV) even after the addition of TBO, suggesting the stability and biocompatibility of synthesized gold-silver core-shell nanoparticles (chit-Au-AgNPs) with TBO.

As presented in Figure.3, the synthesized TBO-chit-Au-AgNPs in the presence of laser irradiation did not exhibit any obvious cytotoxic effects at our tested concentration (0.5 mM). This could be attributed mainly to the biological and chemical properties of chitosan, as well as low toxic effect of TBO on fibroblast cells[17].

One of the main factors responsible for the resistance of *S.aureus* and *P. aeruginosa* to both antibiotics and immune cells is their propensity to form biofilms. We therefore assessed the antibacterial activity of TBO-chit-Au-AgNPs in the presence as well as in the absence of laser irradiation using colony formation assay against polymicrobial biofilms and compared with that of monomicrobial biofilms. A substantial reduction in bacterial load was achieved when monomicrobial and polymicrobial biofilms of S.aureus and P. aeruginosa treated with TBO-chit-Au-AgNPs and subsequently to 100 J/cm^2 of laser irradiation (**Figure.4**). The results from the present study illustrated synergistic interaction between *S.aureus* and *P. aeruginosa* which is in concordance with previous studies[13]. Moreover, we have found Gram-positive, *S. aureus* as more sensitive towards nanoparticle mediated photodynamic therapy as compared to Gram-negative, *P. aeruginosa.* Since, it has been reported in the literature that teichoic acid found within the cell wall of Gram-positive bacteria is the main binding site of some small molecules and nanoparticles[18].

In order to illustrate the above outcomes, we further analyzed the mechanism behind the antibacterial activity of TBO-chit-Au-AgNPs mediated photodynamic therapy using DCFH-DA and quantified the production of total reactive oxygen species (ROS) under laser irradiation. Our data showed increase production of intracellular ROS in TBO-chit-Au-AgNPs mediated photodynamic therapy treated group as compared to TBO-chit-Au-AgNPs alone, both in monomicrobial as well as in polymicrobial biofilms. Additionally, bacterial cells have

sufficient amount of scavengers such as catalase, peroxidase and superoxide dismutase to thwart the free radical mediated bactericidal activity, however they have no remedy against the singlet oxygen molecule, as a result, 1O2 leads to maximum cell damage19. Therefore, to confirm the type of phototoxicity, we have used AMDA. Our data revealed enhanced production of 1O2 in TBO-chit-Au-AgNPs mediated PDT treated group as compared to control and only TBO-chit-Au-AgNPs treated groups (**Figure.5 d,e,f**).

Furthermore, the ability of bacterial adherence and exopolysaccharide production which are significantly important for the formation of biofilm architecture, were analyzed by Crystal violet (CV) and Congo red (CR)-binding assays, respectively. Our data revealed polymicrobial biofilm was more impervious and difficult to eradicate than monomicrobial biofilm[20] (**Figure.6**). This may be due to the presence of more than one type of EPS formed by the bacteria which resulted into more viscous matrix[21].

CLSM micrographs illustrate disruption of polymicrobial biofilms of S.aureus and P. aeruginosa in TBO-chit-Au-AgNPs mediated photodynamic therapy treated group as compared to control and exclusively TBO-chit-Au-AgNPs treated groups. Moreover, the monomicrobial biofilms of S. aureus and P. aeruginosa was found to be more severely disrupted, almost all the bacterial cells in the biofilms were found dead in TBO-chit-Au-AgNPs mediated PDT group, as compared to control and exclusively TBO-chit-Au-AgNPs treated group (Figure.7). Thereby, demonstrating strong antibiofilm action of TBO-chit-Au-AgNPs mediated photodynamic therapy. This observation was further supported by the scanning electron microscopy.

Our result showed that daily topical exposure of TBO-chit-Au-AgNPs followed by light irradiation led to marked reduction of S. aureus and P. aeruginosa colonization in diabetic foot ulcer rats (Figure.9). Previous study has shown that foot ulcers in the diabetic rats healed slower than those of the non-diabetic rats, however in the present study, TBO-chit-Au-AgNPs mediated PDT remarkably healed foot ulcer in diabetic rats within 7 days, after daily treatment (Figure.10, 11 A, B, C). Such fast recovery might obviate the chances of having further bacterial infection and consequent mortality. Furthermore, the result of histopathological investigation of monomicrobial and polymicrobial DFU revealed that TBO-chit-Au-AgNPs mediated PDT promotes healing and reduces inflammation in DFU rats.

Foot ulcers in diabetic patients take a long time to heal due to a series of cellular and molecular mechanism employed in the process of healing, such as neuropathy, high probability of infection, non-physiological inflammatory response, lack of neoangiogenesis, oxidative stress, insufficient concentrations of growth factors, cellular abnormalities, etc.1, 32. We have shown decreased levels of IL-6 and TNF-α in TBO-chit-Au-AgNPs mediated photodynamic therapy treated groups as compared to control, untreated and only TBO-chit-Au-AgNPs treated groups, implying restoration of immunosuppression (Figure. 12-a and **b**). Furthermore, we have found higher levels of EGF and VEGF in all those groups of rats whose ulcers healed as compared to those groups whose ulcers did not healed (**Figure. 12-c and d**). This might be, because EGF promote ulcer healing by stimulating cell growth, proliferation and differentiation whereas, VEGF stimulates vasculogenesis and angiogenesis23,24. Besides this, elevated level of TGF-β-1 was found in all diabetic groups (with and without foot ulcer) (**Figure.12e**). This is because TGF-β-1 is a systemic marker of type-2 diabetes and is positively associated with hyperglycemia. In addition, IGF-1 level was found to be lower in diabetic rats as compared to

non-diabetic and control rats. However, considerable decrease was found in DFU rats with polymicrobial infections (**Figure.12f**). IGF-1 contributes in cell granulation during wound healing; its expression decreases in diabetic patients which resulted into anomalies in cell granulation[25].Thus, the findings of present study clearly indicate pathogenesis, healing of DFU and infection control.

Methodology:

Nanoparticles synthesis

Chitosan coated gold nanoparticles termed as 'core' was synthesized by mixing 15 ml of 10 x 10^{-3} M (10 mM) $HAuCl_4$ and 90 ml chitosan solution under magnetic stirring at 50°C. The appearance of a red color indicates the formation of spherical gold nanoparticles. The next step involves 3 consecutive additions of 140 µl of 10 x 10^{-1} M of $AgNO_3$ to a solution containing 70 ml of chit-AuNPs and 560 µl of 10 x 10^{-1} M of ascorbic acid, the latter used as reducing agent in this mixture.

Characterization

UV-visible spectrophotometer was used to measure the mode of interaction of chit-Au-AgNPs (0.5 mM) with TBO (1 mg ml^{-1}). Transmission electron microscope was employed to observe the size and morphology of the nanocomposites. Scanning electron microscopy (SEM) with energy dispersive X-ray spectrometry (EDS) were carried out to verify the presence of gold and silver. Hydrodynamic size and zeta potential of chit-AuNPs, chit-Au-AgNPs and TBO-chit-Au-AgNPs were recorded using Malvern Zetasizer (Nano ZS, Malvern, UK).

Bacterial strains and culture condition

S. aureus and *P. aeruginosa* were used in this study. Brain Heart Infusion (BHI) broth was used to culture bacteria at 37 °C for 24 hours.

Photosensitization and light source

Red diode laser was used for photosensitization.

The samples acquire the shape of a hemisphere; hence the irradiated area was $2\pi r^2$, where r is the radius of the laser beam exposed, which is equal to 0.35 cm. The beam height from the base was 24.8 mm. Thus, the value of applied PD was 0.1300 Wcm^{-2} and the energy fluency was set to 100 Jcm^{-2} (12 minutes and 50 seconds) based on above mentioned formula.

Estimation of *in vitro* antibacterial activity by colony forming assay

Staphylococcus aureus and *Pseudomonas aeruginosa* were grown overnight in BHI broth supplemented with 1% sucrose. Thereafter, the cell densities of the suspensions were adjusted to approximately 10^8 CFU/mL using spectrophotometer. 100µl of the diluted bacterial suspension were added into 96 well plates and incubated for 24 hours at 37ºC. Subsequently, the preformed biofilm was incubated with TBO-chit-Au-AgNPs in the dark for 30 min and then irradiated with 100 J/cm2 (12 minutes and 50 seconds). Control (matured biofilm in phosphate buffer saline) and only TBO-chit-Au-AgNPs treated wells were not exposed to laser light. Finally, the resulting biofilm was then disrupted by vortexing followed by 10-fold serial dilution. 100 µl of the diluted suspension was spread onto BHI agar plate and then incubated at 37ºC for 24 h.

Total ROS detection inside the cells

2′, 7′- dichlorofluorescein-diacetate (DCFH-DA) was used to quantify endogenous ROS production in biofilms. Monomicrobial and polymicrobial *S. aureus* and *P. aeruginosa* biofilms were grown for 24 h as described above. After incubation, the cultures were centrifuged at 10,000 x g for 15 min. Pellets were washed two times with PBS and finally re-suspended in it by adjusting the cell density to 108 CFU/ml followed by incubation for 10

minutes with 10 μM DCFH-DA. At the end of incubation, the cells were treated with TBO-chit-Au-AgNPs and then irradiated with or without laser light. In, only light treated group, cells were exposed to 100 J/cm2 of laser light. Thereafter, the fluorescence intensity produced from DCFH-DA was estimated by excitation at 485 nm using slit width 1.5 nm35.

Evaluation of singlet oxygen in biofilms

9, 10-Anthracenediylbis (methylene) dimalonic acid (AMDA) was employed to quantify the 1O2 quantum yields of TBO-chit-Au-AgNPs with and without laser light treatment.

10 μM AMDA was added to the solutions containing monomicrobial and polymicrobial *S. aureus* and *P. aeruginosa* (10^8 CFU/ml) biofilms in PBS followed by the treatment as explained above. The reduction in the 399-nm absorption peak of AMDA after treatment corresponds to the amount of singlet oxygen produced.

Quantification of biofilm formation by crystal violet assay

Crystal violet assay was performed to quantify the biomass of the monomicrobial and polymicrobial biofilms after treatment with TBO-chit-Au-AgNPs mediated photodynamic therapy. Preformed monomicrobial and polymicrobial biofilms of *S. aureus and P. aeruginosa* were grown for 24 hours as described in colony forming assay. Thereafter, the biofilm was incubated with TBO-chit-Au-AgNPs mediated for 30 mins and then exposed to laser light (100 J/cm2). Subsequently, the control and treated (only TBO-chit-Au-AgNPs treated, TBO-chit-Au-AgNPs + laser light treated) wells of microtiter plates were fixed with formalin (37%, diluted 1:10) and 2% sodium acetate. Biofilms in different groups were stained with 200μl of crystal violet (0.1%, 15 min). Thereafter, plates were shaken for 10 min to allow full release of the dye and the absorbance was recorded at 630 nm[35].

Congo red (CR)-binding assay

The Congo red (CR)-binding assay was conducted to estimate the production of exopolysaccharide (EPS), as reported earlier. Same treatment was given on the preformed biofilm as described above. Thereafter, the exhausted media was removed and wells were washed with PBS twice. 100 µl of fresh medium and 50 µl of CR (0.5 mM) were added into each well containing control and treated samples. The mixture solution of fresh medium (100 µl) and CR (50 µl) was also used for blank measurements (blank CR). Subsequently, the microtiter plate was incubated for 2 hours at 37 °C. The supernatants were collected and color change was measured at 490 nm[42].

Live/Dead Staining by CLSM

Confocal laser scanning microscopy (CLSM) was performed to analyze the consequence of nano photodynamic therapy on monomicrobial and polymicrobial biofilm formation by *S. aureus* and *P. aeruginosa*. Biofilm was grown in covered glass bottom confocal dishes for 24 h at 37 °C. The adhered cells or the preformed biofilm was treated as describe above, while controls were left untreated. Then, the biofilm was stained with propidium iodide (PI) and syto9 followed by incubation at 37ºC for 1 h.

Structural imaging of bacteria in biofilms

Scanning electron microscopy (SEM) was executed to observe the morphology of *S. aureus* and *P. aeruginosa* monomicrobial as well as polymicrobial biofilms after treatment with TBO-chit-Au-AgNPs followed by exposure to laser light. After treatment, biofilms in each sample were fixed with 2% formaldehyde + 2.5% glutaraldehyde in PBS for 2 h at 4ºC. The fixed samples were serially dehydrated with different concentrations of ethanol (20%, 40%, 60%, 80%, and 100 %).

Cytotoxicity Assay

A cytotoxicity assay was performed on L929 fibroblast cells. Cells (~10^5cells/well) were seeded in 96-well plates, left overnight to adhere and then treated with various concentrations (0.25 mM, 0.5 mM and 1 mM) of TBO-chit-Au-AgNPs in the presence as well as in the absence of laser irradiation. After 24 h, cell viabilities were determined by methyl thiazolyl tetrazolium (MTT) assay. The medium was removed, and 100 µl of the mixture solution containing fresh medium and MTT (5 mg/ml) solution was added into each well, followed by incubation for 4 h at 37ºC. Subsequently, the formazan crystals formed by the reduction of MTT, were dissolved in DMSO and the absorbance was quantified.

***In vivo* study**

A total of 56 adult male wistar rats, weighing, 250-300g, were used in this study. The rats were equally divided into 6 main groups. Each group and sub-groups consisted of 4 rats each. Group 1 consisted of normal rats without type 2 diabetes mellitus (DM) and foot ulcer (Control); Group 2 contained rats with DM (Untreated); Group 3 consisted of rats with foot ulcer (Untreated); Group 4 contained rats with diabetic foot ulcer (Untreated); Group 5 consisted of diabetic foot ulcer rats treated with TBO-chit-Au-AgNPs while group 6 contained diabetic foot ulcer rats treated with TBO-chit-Au-AgNPs + laser light (100 J/cm^2).

Experimental induction of diabetes

The animals were fasted overnight and diabetes was induced by a single intra-peritoneal injection of a freshly prepared solution of streptozotocin (40 mg/kg b. wt) in 0.1 M citrate buffer (pH 4.5)[1]. Control rats were injected with citrate buffer only. The rats were kept for 14 days to stabilize the diabetic condition.

Foot Ulceration

Induction of foot ulcer was based on an excisional model. Rats with a blood glucose level greater than 300 mg/dl were used for foot ulceration. On the day of foot ulceration (Day 0), each rat was anesthetized by intraperitoneal injections of ketamine/xylazine cocktail. A 2 mm x 5 mm rectangular full thickness ulcer was created in the skin of the footpad on the right hind leg of each rat using a scalpel.

Treatment of DFU by nano-photodynamic therapy

The infected foot ulcers were irradiated daily in morning time for 1 week, starting on the 3rd day post infection induction. TBO-chit-Au-AgNPs was added in the middle and spread over the whole infected area. Thirty minutes after the addition, irradiation was carried out with 630 nm of laser light for 12 minutes and 50 seconds which corresponds to 100 J/cm^2.

Determination of bacterial load reduction (CFU/ml)

In order to confirm the absence of monomicrobial and polymicrobial *S. aureus* and *P. aeruginosa* colonization, bacterial load was measured for every sample by CFU counting on BHI agar plates and expressed as CFU per ml. Collected samples were serially diluted and plated onto BHI agar plates to determine the number of bacteria. The plates were incubated at 37°C for 24 hours before enumeration of colonies.

Histopathological analysis

Fresh skin biopsies of control, untreated and treated rat groups were incised and fixed in 10 % phosphate buffered formalin (pH 7.4). The tissues were then dehydrated in ascending grades of ethyl alcohol, cleared in xylene and mounted in molten paraplast at 58-62°C. Thereafter, 5-µm histological sections were cut and stained with haematoxylin and eosin (H/E) to examine microorganism response.

Effects of nano-photodynamic therapy on growth factors and inflammatory cytokines involved in the pathogenesis of diabetic foot ulcers

To determine the production level of growth factors and inflammatory cytokines, blood samples were drawn under anesthesia and collected into sterile blood collection tubes from the eyes of controls rats, untreated rats, only TBO-chit-Au-AgNPs treated rats and TBO-chit-Au-AgNPs + laser light treated rats. Rats were immediately sacrificed as per the guidelines. The samples were centrifuged at 5000 rpm for 5 min. Thereafter, the serum supernatant was aliquoted in microcentrifuge tubes and stored at -80ºC for further analysis. The commercially available enzyme-linked immunosorbent assay (ELISA) kits were used according to the manufacturers' protocol: Rat TNF-α ELISA Kit, Rat IL-6 ELISA Kit, Rat TGF-β1 ELISA Kit, Rat EGF ELISA Kit, Rat VEGF-A ELISA Kit, Rat IGF-1 ELISA Kit. The levels of TNF-α, IL-6, TGF-β1, EGF, VEGF-A and IGF-1 were measured by ELISA reader.

Conclusion

We have developed a stable and biocompatible chitosan coated gold-silver core shell nanoparticles conjugated with TBO. The synthesized TBO-chit-Au-AgNPs mediated photodynamic therapy was used for the first time to eliminate multi-drug resistant Gram-positive, and Gram-negative, monomicrobial as well as polymicrobial biofilms. Furthermore, this novel nano-phototheranostic complex proved as a nontoxic antibacterial agent to combat DFU caused by multi-drug resistant bacterial strains. Therefore, this approach holds a promising potential to be validated and implemented in clinical translation.

Note: Human trials has been approved by ICMR reference no: CTRI / 2023/05/052838 which is supported by BIG BIRAC Grant and has been initiated on 30 Human subject after ethical approval.

References

1. Yu, Caroline Oi-Ling, Kwok-Sui Leung, Kwok-Pui Fung, Francis Fu-Yuen Lam, Ethel Sau-Kuen Ng, Kit-Man Lau, Simon Kwoon-Ho Chow, Wing-Hoi Cheung. The characterization of a full-thickness excision open foot wound model in n5-streptozotocin (STZ)-induced type 2 diabetic rats that mimics diabetic foot ulcer in terms of reduced blood circulation, higher C-reactive protein, elevated inflammation, and reduced cell proliferation. *Experimental animals* **2017**, 66, no. 3: 259-269.
2. Falanga, Vincent. Wound healing and its impairment in the diabetic foot. *The Lancet* **2005**, 366, no. 9498: 1736-1743.
3. Kwon, Ki Tae, David G. Armstrong. Microbiology and antimicrobial therapy for diabetic foot infections. *Infect. Chemother.* **2018**, 50, no. 1: 11.
4. De la Fuente-Núñez, César, FanyReffuveille, Evan F. Haney, Suzana K. Straus, Robert EW Hancock. Broad-spectrum anti-biofilm peptide that targets a cellular stress response. *PLoSPathog.***2014**, 10, no. 5: e1004152.
5. Lipsky, Benjamin A., Anthony R. Berendt, H. Gunner Deery, John M. Embil, Warren S. Joseph, Adolf W. Karchmer, Jack L. LeFrock. Diagnosis and treatment of diabetic foot infections. *Clin. Infect. Dis.* **2004**, 885-910.
6. Stacy, Apollo, Luke McNally, Sophie E. Darch, Sam P. Brown, Marvin Whiteley. The biogeography of polymicrobial infection. *Nat. Rev. Microbiol.* **2016**, 14, no. 2: 93-105.
7. Ferrer-Espada, Raquel, Xiaojing Liu, Xueping Sharon Goh, Tianhong Dai. Antimicrobial blue light inactivation of polymicrobial biofilms. *Front. Microb.* **2019**, 10:721.
8. De Leon, Stephanie, Allie Clinton, Haley Fowler, Jake Everett, Alexander R. Horswill, Kendra P. Rumbaugh. Synergistic interactions of Pseudomonas aeruginosa and

Staphylococcus aureus in an in vitro wound model. *Infect. Immun.* **2014**, 82, no. 11: 4718-4728.

9. Nguyen, Angela T., Amanda G. Oglesby-Sherrouse. Interactions between Pseudomonas aeruginosa and Staphylococcus aureus during co-cultivations and polymicrobial infections. *Appl. Microbiol. Biotechnol.* **2016**, 100, no. 14: 6141-6148.

10. Parveen, Suphiya, RanjitaMisra, Sanjeeb K. Sahoo. Nanoparticles: a boon to drug delivery, therapeutics, diagnostics and imaging. *Nanomedicine: Nanotechnology, Biology and Medicine* **2012**, 8, no. 2: 147-166.

11. Salem, Dina S., Mahmoud A. Sliem, Mohamed El-Sesy, Samia A. Shouman, Yehia Badr. Improved chemo-photothermal therapy of hepatocellular carcinoma using chitosan-coated gold nanoparticles. *J. Photochem. Photobiol., B* **2018**, 182: 92-99.

12. Hada, Alexandru-Milentie, Monica Potara, SorinaSuarasan, Adriana Vulpoi, Timea Nagy-Simon, Emilia Licarete, SimionAstilean. Fabrication of gold–silver core–shell nanoparticles for performing as ultrabright SERS-nanotags inside human ovarian cancer cells. *Nanotechnol.* **2019**, 30, no. 31: 315701.

13. 1Sondi, Ivan, BrankaSalopek-Sondi. Silver nanoparticles as antimicrobial agent: a case study on E. coli as a model for Gram-negative bacteria. *J. Colloid Interface Sci.* **2004**, 275, no. 1: 177-182.

14. Sharma, Mrinalini, Livia Visai, Francesca Bragheri, Ilaria Cristiani, Pradeep Kumar Gupta, Pietro Speziale. Toluidine blue-mediated photodynamic effects on staphylococcal biofilms. *Antimicrob. Agents Chemother.* **2008**, 52, no. 1: 299-305.

15. Khan, Shakir, Shahper N. Khan, Ramovatar Meena, Ayaz M. Dar, Ruchita Pal, Asad U. Khan. Photoinactivation of multidrug resistant bacteria by monomeric methylene blue conjugated gold nanoparticles. *J. Photochem. Photobiol., B* **2017**, 174: 150-161.

16. Lu, Lu, Gwendolyn Burkey, IonelHalaciuga, Dan V. Goia. Core-shell gold/silver nanoparticles: Synthesis and optical properties. *J. Colloid Interface Sci.* **2013**, 392: 90-95.

17. Kumar, MNV Ravi, RA Muzzarelli, C. Muzzarelli, H.Sashiwa, A.J. Domb. Chitosan chemistry and pharmaceutical perspectives. *Chem. Rev.* **2004**, 104.12: 6017-6084.

18. Caudill, Emily R., Rodrigo Tapia Hernandez, Kyle P. Johnson, James T. O'Rourke, Lingchao Zhu, Christy L. Haynes, Z. Vivian Feng, and Joel A. Pedersen. Wall teichoic acids govern cationic gold nanoparticle interaction with Gram-positive bacterial cell walls. *Chemical Science* 11, **2020,** 16 : 4106-4118.

19. , Kim, Sun Yee, Ok Jung Kwon, Jeen-Woo Park. Inactivation of catalase and superoxide dismutase by singlet oxygen derived from photoactivated dye, *Biochimie***2001**, 83, no. 5 437-444.

20. Pereira, Cristiane Aparecida, Rogerio Lima Romeiro, Anna Carolina Borges Pereira Costa, Ana Karina Silva Machado, Juliana Campos Junqueira, Antonio Olavo Cardoso Jorge. Susceptibility of Candida albicans, Staphylococcus aureus, and Streptococcus mutans biofilms to photodynamic inactivation: an in vitro study. *Lasers in medical science* **2011**, 26 no.3: 341-348.

21. Skillman, L. C., I. W. Sutherland, M. V. Jones. The role of exopolysaccharides in dual species biofilm development. *J. Appl. Microbiol.* **1998**, 85.S1: 13S-18S.

22. Vlassara, Helen, Yong Ming Li, Farhad Imani, Donald Wojciechowicz, Zhi Yang, Fu-Tong Liu, Anthony Cerami. Identification of galectin-3 as a high-affinity binding protein for

advanced glycation end products (AGE): a new member of the AGE-receptor complex. *Mol. Med.* **1995**, 1, no.6: 634-646.

23. Ojalvo, Ariana García, Jorge Berlanga Acosta, Yssel Mendoza Mari, Maday Fernandez Mayola, Calixto Valdes Perez, William Savigne Gutierrez, IIeydis Iglesias MarichalSeijas, EA, Kautzman, A.M., Pacheco, A.E., Armstrong , D.G. Healing enhancement of diabetic wounds by locally infiltrated epidermal growth factor is associated with systemic oxidative stress reduction. *International wound journal***2017**, 14. no.1: 214-225.

24. Gardner, Jason C., Huixing Wu, John G. Noel, Benjamin J. Ramser, Lori Pitstick, Atsushi Saito, Nikolaos M. Nikolaidis, Francis X. Mc Cormack. Keratinocyte growth factor supports pulmonary innate immune defense through maintenance of alveolar antimicrobial protein levels and macrophage function. *Am. J. Physiol. Lung Cellular and Molecular Physiology***2016**, 310, no. 9: L868-L879.

25. Zubair, Mohammad, Jamal Ahmad. Role of growth factors and cytokines in diabetic foot ulcer healing: a detailed review. *Rev. Endocr. Metab. Disord.* **2019**, 20, no.2: 207-217.

Table 1. Hydrodynamic diameter (size by number) obtained from DLS, Polydispersity index (PDI) and zeta potential values of chit-AuNPs, chit-Au-AgNPs and TBO-chit-Au-AgNPs.

Sample	Size (d.nm)	Polydispersity index (PDI)	Zeta potential (mV)
chit-AuNPs	**129.4**	**0.107**	**49**
chit-Au-AgNPs	**131**	**0.067**	**37.6**
TBO-chit-Au-AgNPs	**134**	**0.085**	**41.2**

Table 2. Experimental induction of type-2 diabetes by streptozotocin (STZ) injection.

S.No.	Groups	Blood sugar concentration (mg/dL) in overnight fasting rats before the injection of Streptozotocin (STZ)	Blood sugar concentration (mg/dL) after the injection of Streptozotocin (STZ)
1.	Control (normal rats)	i. 102 ii. 92 iii. 87 iv. 108	-
2.	Diabetic without ulcer (untreated rats)	i. 98 ii. 90 iii. 89 iv. 99	i'. 368 ii'. 239 iii'. 366 iv'. 261
3.	*Pseudomonas aeruginosa* Diabetic with ulcer (untreated rats)	i. 110 ii. 102 iii. 94 iv. 87	i'. 325 ii'. 338 iii'. 302 iv'. 319

4.	*Pseudomonas aeruginosa* Diabetic with ulcer (TBO-chit-Au-AgNPs treated rats)	i. 95 ii. 130 iii. 94 iv. 102	i'. 380 ii'. 397 iii'. 394 iv'. 382
5.	*Pseudomonas aeruginosa* Diabetic with ulcer (TBO-chit-Au-AgNPs +light treated rats)	i. 108 ii. 100 iii. 80 iv. 98	i'. 376 ii'. 265 iii'. 277 iv'. 264
6.	*Staphylococcus aureus* Diabetic with ulcer (untreated rats)	i. 138 ii. 112 iii. 98 iv. 104	i'. 309 ii'. 386 iii'. 287 iv'. 312
7.	*Staphylococcus aureus* Diabetic with ulcer (TBO-chit-Au-AgNPs treated rats)	i. 139 ii. 87 iii. 94 iv. 93	i'. 299 ii'. 310 iii'. 264 iv'. 317
8.	*Staphylococcus aureus*	i. 130 ii. 123 iii. 117	i'. 385 ii'. 305 iii'. 377

	Diabetic with ulcer (TBO-chit-Au-AgNPs +light treated rats)	iv. 103	iv'. 338
9.	Polymicrobial (*Staphylococcus aureus* + *Pseudomonas aeruginosa*) Diabetic with ulcer (untreated rats)	i. 104 ii. 110 iii. 96 iv. 117	i'. 291 ii'. 271 iii'. 359 iv'. 331
10.	Polymicrobial (*Staphylococcus aureus* + *Pseudomonas aeruginosa*) Diabetic with ulcer (TBO-chit-Au-AgNPs treated rats)	i. 109 ii. 106 iii. 103 iv. 122	i'. 362 ii'. 358 iii'. 376 iv'. 321
11.	Polymicrobial (*Staphylococcus aureus* + *Pseudomonas aeruginosa*) Diabetic with ulcer (TBO-chit-Au-AgNPs +light treated rats)	i. 106 ii. 114 iii. 73 iv. 111	i'. 319 ii'. 375 iii'. 332 iv'. 345

Asad Ullah Khan